Effect of doping concentration on electronic, magnetic and optical properties of (Fe, Mn) co-doped $SrTiO_3$: A first-principles study

YUEQIN WANG[a,b], YIN LIU[a,*], QIAN ZHAI[a], MINGXU ZHANG[a]
[a]*School of Material Science and Engineering, Anhui University of Science and Technology, Huainan 232001, China*
[b]*School of Mechanics and optoelectronic Physics, Anhui University of Science and Technology, Huainan 232001, China*

The electronic structure, magnetic and optical properties of (Fe, Mn) co-doped $SrTiO_3$ with varying doping concentrations are investigated using first-principles calculation. The results show that there exhibits an antiferromagnetic (AFM) to ferromagnetic (FM) phase transition with increasing doping concentration. The $SrTi_{1-2x}Fe_xMn_xO_3$ shows a magnetic half-metallic character with the doping concentration x = 0.25, which is ascribed to the excitation of the O-2p states into the conduction band. The optical absorption spectra of codoped STO show obvious red-shift after doping, indicating that it could be taken as a potential candidate for optoelectronic materials.

(Received September 19, 2017; accepted October 10, 2018)

Keywords: $SrTiO_3$, Doping concentration, Magnetic, Optoelectronic

1. Introduction

Recently, perovskite Ti oxide has attracted great attention for potential applications in electronics, optoelectronics, photocatalyst and energy storage [1-3]. $SrTiO_3$ (STO) is one of them. It is known that the pure STO is an insulator with a wide band gap about 3.2 eV or 3.4 eV, and showing a nonferromagnetic behavior [4-6]. However, the drawback of wide band gap has limited its practical application. Many experimental and theoretical works have been carried out to explore room temperature ferromagnetism and new half-metallic materials based on STO [7-10]. It is found that the STO doped with various transition metal (TM) atom, such as Fe, Mn, Cr and Co, is an efficient way to obtain room temperature ferromagnetism [11-15]. Karaphun et al. [15] found that the Fe-doped STO shows ferromagnetic (FM) behavior with increasing Fe content. In theoretical, the bulk Mn is antiferromagnetic (AFM) and the Mn cluster is FM [16,17]. Recently, Choudhury et al. [18] demonstrated that Mn-doped STO is a paramagnetic insulator with greatly dielectric properties, while without finding weak ferromagnetic. Shen et al. [19] reported that (Fe, Mn) co-doped STO to be AFM spin ordering at room temperature with the doping concentration x = 0.037, but without half-metallic character. Since the half-metallic character is useful for optoelectronic applications, it is expected to achieve the half-metallic behavior by codoping with various transition metal atoms and increasing doping concentration. Additionally, precious studies have confirmed that there exhibits hybridization between the 3d impurity states and the near neighbor O-2p states, which induces magnetization in doped STO [19,20]. In order to find half-metallic and ferromagnetic character, it is necessary to investigate the electronic, magnetic and optical properties of (Fe, Mn) co-doped STO with increasing doping concentration.

Therefore, in this paper, the electronic, magnetic and optical properties of (Fe, Mn) co-doped STO are performed by spin-polarized first-principles study. The main purpose of our work is to present ferromagnetic character and bring out half-metallic behavior of (Fe, Mn) co-doped STO. The effects of various positions for the two Ti replaced by the one Fe and one Mn are simultaneously considered. The results show that the Fe and Mn atoms prefer to occupy the nearest neighbor position. So we only present the results of the substitute of nearest neighbor position for Fe and Mn (see Fig. 1). The results of the present work imply that (Fe, Mn) co-doped STO exhibits a AFM to FM transition with increasing the doping concentration, meanwhile, the half-metallic character is found as the doping concentration increases to x = 0.25. The calculated results imply that (Fe, Mn) co-doped STO is likely to be a potential magneto-optical and semiconductor spintronics materials.

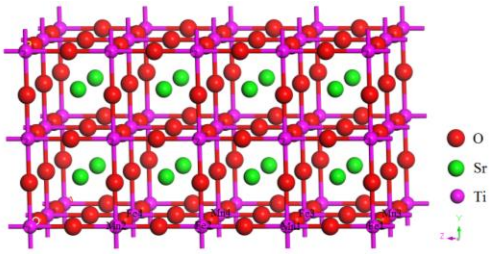

Fig. 1. The 2×2×4 supercell structure of pure STO in the Pm3m space group within 80 atoms. The different sites of Ti atoms replaced by the Fe atoms and Mn atoms are labeled

2. Calculation method

All of the calculations have been carried out by using the CASTEP code within MS8.0 package, which uses the plane-wave pseudo-potential total energy calculation method based on the density functional theory (DFT) [21]. The generalized gradient approximation (GGA) parameterized by perdew-Burke-Ernzerhof is adopted for the exchange-correlation functional. We use U_{eff} = 4 eV on Fe-3d and Mn-3d states for a better description of the localized transition, and it provides a reasonable magnetic structure [22,23]. The basis was treated with Sr $4s^2 4p^6 5s^2$, Ti $3d^2 4s^2$, Fe $3d^6 4s^2$, Mn $3d^5 4s^2$ and O $2s^2 2p^4$. The spin-polarized calculations are adopted to properly describe the total energy and electronic structures of (Fe, Mn) co-doped $SrTiO_3$ system. The energy cutoff is set to 380 eV to ensure convergence, and structure relaxation is carried out until the maximum atomic force within 0.03 eV/Å and the total energy convergence is less than 1×10^{-5} eV/atom. The Brillouin zone integration for the pure and doped $SrTiO_3$ are performed with 8×8×8 and 3×3×2 Monkhorst-Pack *k*-point mesh, respectively.

The optical absorption coefficient $\alpha(\omega)$ [24] is described by

$$\alpha(\omega)=\sqrt{2}\omega\left[\sqrt{\varepsilon_1(\omega)^2+\varepsilon_2(\omega)^2}-\varepsilon_1(\omega)\right]^{1/2}=2\omega k(\omega) \tag{1}$$

where ε_1 and ε_2 are the real and imaginary parts of dielectric function, ω is angular frequency of phonon and $k(\omega)$ is extinction coefficient. The refractive index [25] is evaluated by

$$n(\omega)=\frac{1}{\sqrt{2}}\left[\sqrt{\varepsilon_1(\omega)^2+\varepsilon_2(\omega)^2}+\varepsilon_1(\omega)\right]^{1/2} \tag{2}$$

The absorption coefficient $\alpha(\omega)$ is mainly contributed by the imaginary part $\varepsilon_2(\omega)$. The imaginary part $\varepsilon_2(\omega)$ is calculated from the momentum matrix elements between the occupied and unoccupied wave functions and given by

$$\varepsilon_2(\omega)=\frac{4\pi^2}{\omega^2\Omega}\sum_{j\in CB}^{i\in VB}\sum_k w_k\left|p_{ji}^a\right|^2\delta(\varepsilon_{kj}-\varepsilon_{ki}-\omega) \tag{3}$$

in which Ω is the unit-cell volume and p_{ji}^a are the dipolar transition matrix elements, and *CB* and VB denote the conduction and valence bands, respectively. The real part $\varepsilon_1(\omega)$ can be calculated by the Kramers-Krong transformati- on

$$\varepsilon_1(\omega)=1+\frac{2}{\pi}P\int_0^\infty \mathrm{d}\,\omega\frac{\omega'\varepsilon_2(\omega')}{\omega'^2-\omega^2} \tag{4}$$

where *P* is the principle value of integral.

3. Results and discussion

Pure STO is a perovskite-type phototcatalyst with space group *Pm*3*m*. To model the (Fe, Mn) co-doped STO bulk with single crystal form, we build a 2×2×4 periodic supercell (80 atoms) based on the optimized primitive cell, and the crystal structure of the STO supercell is shown in Fig. 1. We only consider B-site (Ti) doping in our calculations due to the transition metal prefer to enter the B-site in STO [26]. To simulate the effect of different doping concentration on the doped STO, the eight Ti atoms at different sites substitute by Fe atoms and Mn atoms are considered, and the atomic sites are labeled in Fig. 1.

The calculated magnetic structure, lattice constants and spin band gap of pure STO and doped STO are listed in Table 1. It is found that there exhibits an antiferromagnetic (AFM) to ferromagnetic (FM) phase transition with the doping concentration increases, which can be ascribed to the destruction of charge ordering state and the weakened antiferromagnetic spin coupling. In addition, with the increase of doping concentration, the ferromagnetic becomes stronger. The calculated lattice constants for pure STO is $a = c$ = 3.916 Å, which agree well with the experimental data [27]. For the doped STO, it is found that the phase transition from cubic to tetragonal is produced after doping. The lattice distortion is mainly determined by the radius of doping cations. Thus the phase transition in doped STO can be explained by the fact that the radius of substituting cations (Fe^{4+}: 0.585 Å and Mn^{4+}: 0.53 Å) are both larger than that of Ti^{4+} (0.605 Å), which can generate an off-center displacement in the TiO_6 octahedron structure. There is a lattice expansion in doped STO compared with that of pure STO. When the doping concentration is x = 0.625, the value of c/a is the maximum (c/a = 1.013).

Table 1. The lattice constants of Fe-Mn co-doped $SrTO_3$ with different doping concentration. E_{AFM} and E_{FM} are the total energy of antiferromagnetic and ferromagnetic coupling configurations, respectively

Concen.	$E_{AFM}-E_{FM}$ (eV)	Coupling	*a* (Å)	*c* (Å)	*V* (Å^3)
0	—	NM	3.916	3.916	60.052
0.0625	−0.23	AFM	3.923	3.974	61.061
0.125	0.46	FM	3.932	3.940	60.920
0.1875	0.95	FM	3.932	3.945	61.011
0.25	1.76	FM	3.942	3.948	60.981

To clarify the phase transition from semiconductor to half-metallic in doped STO, we investigate the total density of states (TDOS) of (Fe, Mn) co-doped $SrTiO_3$ within different doping concentration, and the results are shown in Fig. 2. As seen from Fig. 2 (a), the calculated band gap of pure STO is about 2.2 eV, which is smaller than the experimental values of about 3.2 eV. The underestimation of spin band gap is a typical feature of DFT calculation, and the strong self-interaction of the

Ti-3d states can also induce the decrease of band gap. Therefore, we adopted a scissor shift of 1.0 eV in the optical property calculation to compensate the underestimate band gap. After doping, there is a significant DOS differences in doped STO, because the symmetry of the cubic structure is broken. It can be observed that some electronic states are excited in to the band gap, indicating that (Fe, Mn) doped STO possesses a typical p-type conducting character. The interesting feature is that the in-gap electronic states goes deeper in to the conduction band (CB) with the increase of doping concentration. For the doped STO with the doping concentration x = 0.25, there is a half-metallic characteristic with the spin-up DOS is metallic at the Fermi level and the spin-down DOS is insulting with a large band gap about 2.24 eV. The noticeable feature is that some in gap electronic states are found in the spin-up DOS, but not in the spin-down DOS, which induces a net magnetic moment.

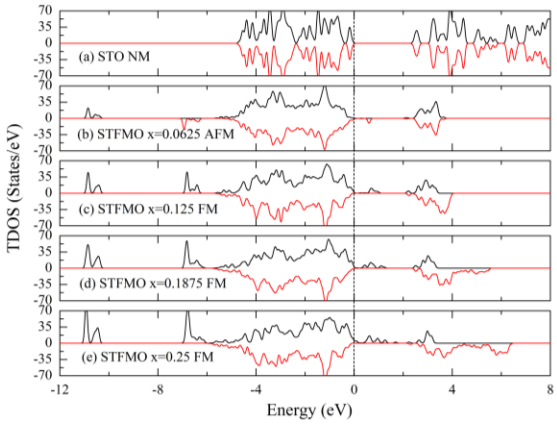

Fig. 2. Total DOS of pure STO (a) and doped $SrTiO_3$ (STFMO) with doping concentration x = 0.0625 (b) x = 0.125 (c) x = 0.1875 (d) x = 0.25 (e)

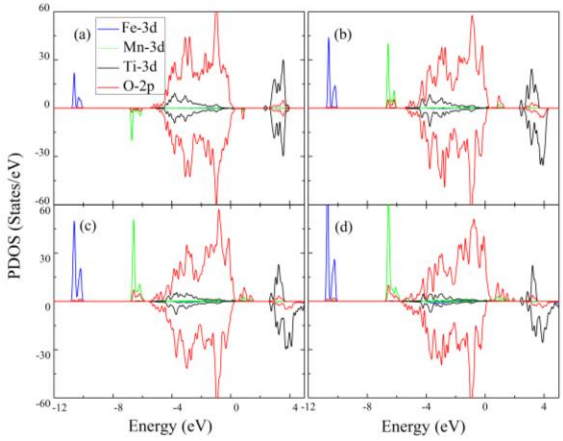

Fig. 3. Partial DOS of (Fe, Mn) co-doped STO with doping concentration x = 0.0625 (a) x = 0.125 (b) x = 0.1875 (c) x = 0.25 (d)

To further investigate the effect of the (Fe, Mn) co-doping on the electronic structure and magnetic property of doped STO, the partial density of states (PDOS) of doped STO are calculated and shown in Fig. 3. From the partial DOS analysis it follws that the in-gap electronic states originate mainly from the O-2p states and the impurity Mn-3d states, which implies that the Mn-O hybridization plays major role in the reduced band gap. In addition, the hybridization between Mn-3d (Fe-3d) states and O-2p states becomes stronger with the doping concentration increases. It is noticeable that the Mn-O hybridization is stronger than that of Fe-O hybridization, indicating that the (Fe, Mn) co-doping makes mainly impact on the magnetic moment of Mn atoms. In contrast, the hybridization between the Ti-3d states and the O-2p states is slightly reduced after doping. As seen from Fig. 3(d), the spin-up DOS passes through the Fermi level, which is ascribed to the O-2p states excite into the CB.

Table 2. The magnetic moment of magnetic atoms with different doping concentration

Concentration	Magnetic moment (μ_B)			
	Fe	Mn	O near Fe1	O near Mn1
0.0625	4.48	3.93	0.10	0.14
0.125	4.39	3.99	0.10	0.14
0.1875	4.33	3.99	0.13	0.15
0.25	4.33	4.01	0.18	0.17

The calculated net magnetic moments of magnetic atoms with different doping concentrations are listed in Table 2. It is found that the doping concentrations make great influences on the magnetic moments of magnetic atoms. It is well known that the theoretical magnetic moments of Fe^{4+} and Mn^{4+} are 4 μ_B and 3 μ_B, respectively, while the calculated magnetic moments of Fe^{4+} and Mn^{4+} in doped STO are larger than the theoretical results. The magnetic moment of Fe^{4+} is decreases with the doping concentration increases, oppositely, the magnetic moment of Mn^{4+} is increases with the doping concentration increases. The noticeable feature is that the calculated magnetic moment of Mn^{4+} is very close to that of Mn^{3+}, which indicate that the co-doping induces the increase of local Mn^{3+} and leads to the enhancement of ferromagnetic double exchange interaction between Mn^{4+} and Mn^{3+}. The magnetic O atoms are present near the Fe and Mn atom, and the calculated magnetic moments of magnetic O atoms near the Fe1 and Mn1 atom are listed in Table 2. It is noticed that the magnetic moment of magnetic O atom is increases with the doping concentration increases, particularly, the magnetic moments of magnetic O atoms are exactly the same as the doping concentration is below 0.125.

The partial DOS of magnetic O atoms near the Fe atom and the Mn atom in doped STO are performed and the results are shown in Fig. 4. From the PDOS as shown in Fig. 4, it can be observed that O-2p states of magnetic O

atom mainly appear in the energy interval from -6.0 to 0 eV. The doping concentrations have great influence on the PDOS of O-2p states near the Fe atoms, which lead to the obvious change in the magnetic moments of Fe atoms. In contrast to these, the PDOS of O-2p states near the Mn atoms are slightly affected by the doping concentrations, which leads to the hybridization between the nearest Mn-3d states and the O-2p states is relatively stable, thus the magnetic moment of Mn changes little. The presence of magnetic moment on O atom is indicative of the hybridization between the O-2p states and the 3d states of magnetic atoms (Fe and Mn). As shown in Fig. 4, the PDOS of O-2p states near the Mn atoms located in CB are much larger than the one near the Fe atoms. As mentioned above, the presence of spin-up density is metallic at Fermi level with the doping concentration up to x = 0.25, which is related to the excitation of the O-2p states, however, it can be followed that the excitation states originate from the magnetic O atoms near the Fe or Mn.

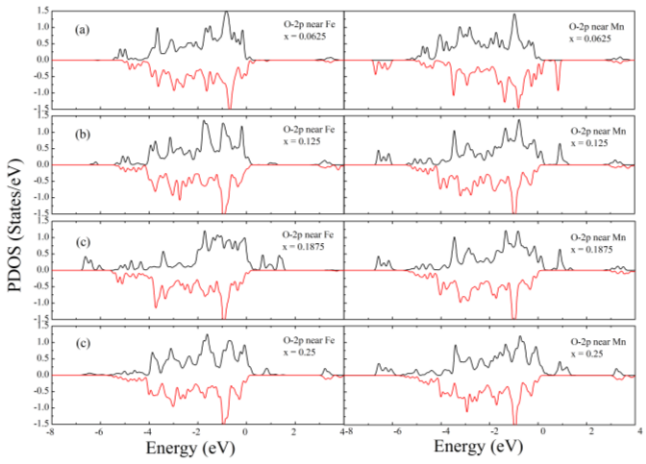

Fig. 4. Partial DOS of the magnetic O atoms near the Fe and Mn atoms with doping concentration x = 0.0625 (a) x = 0.125 (b) x = 0.1875 (c) x = 0.25 (d)

Because the photocatalytic activity only respond to semiconductor character, in the present work we only considered the optical properties of pure STO and doped STO with the reduced band gap behavior (x = 0, 0.0625, 0.125, 0.1875). Since the refractive index $n(\omega)$ and extinction coefficient $k(\omega)$ are proportional to the real and imaginary part of dielectric function, which indicates that the two spectra are similar, here we only discuss the refractive index and extinction coefficient of pure STO and doped STO in semiconductor character. The refractive index $n(\omega)$ and extinction coefficient $k(\omega)$ are calculated and shown in Fig. 5. As shown in Fig. 5, the calculated refractive index $n(\omega)$ and extinction coefficient $k(\omega)$ of STO are agreement with the experimental results, and the doping concentration has a great influence on the optical properties of STO [28]. As seen from Fig. 5(a), the calculated static refractive index $n(0)$ of doped STO are 1.84 eV, 2.18 eV and 2.52 eV for the doping concentration x = 0.0625, 0.125 and 0.1875, respectively. It is found that the $n(0)$ of doped STO is increases with the doping concentration increases. In addition, the value of $n(0)$ with doping concentration x = 0.125 is very close to that of the experimental data ($n(0)$ = 2.17) of pure STO. There is a energy shift of $n(\omega)$ for the two refractive peaks, and the both are shift to the lower energy range. As seen from Fig. 5(b), the absorption edge of extinction coefficient $k(\omega)$ starts at about 2.48 eV and 0.23 eV for pure STO and doped STO, respectively. It can be noticed that the $k(\omega)$ spectra of doped STO have much sharper peaks in the lower energy range, which is ascribed to the great difference of the electronic structure between the pure STO and the doped STO. As mentioned above, the stronger Mn-O covalent bond leads to a reduced band gap, additionally, the smaller band gap in doped STO is play a major role in the shift of the peaks of optical spectra to the lower phonon energy region.

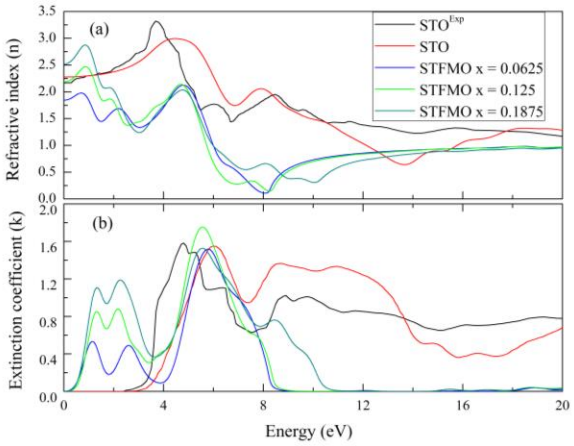

Fig. 5. Refractive index n(ω) (a) and extinction coefficient k(ω) (b) of pure STO and doped STO (STFMO) with different doping concentration

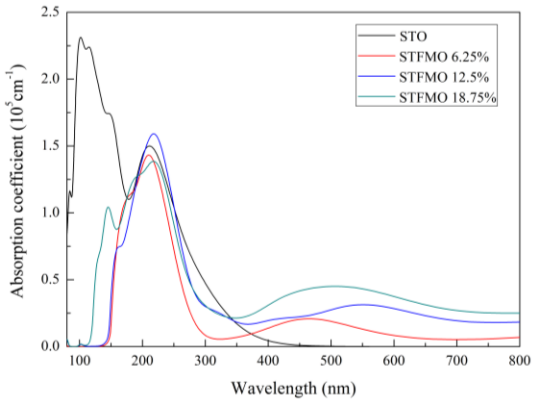

Fig. 6. Absorption coefficient for pure STO and doped STO (STFMO) with different doping concentration

Additionally, the optical absorption coefficient $\alpha(\omega)$ of pure STO and doped STO are performed and the results are shown in Fig. 6. For the pure STO, our calculated $\alpha(\omega)$

agrees well with experimental results [29]. It can readily identified two characteristic peaks at about 102 nm and 211 nm for pure STO. There is an obvious red shift of the absorption spectra edge after doping, which is contribute to the high photocatalytic activities of doped STO. When the doping concentration increases to x = 0.125, the two characteristic peaks are shift to 219 nm and 551 nm, respectively. It is interesting to find that the two peaks move to the short wavelength direction with the increasing doping concentration up to x = 0.1875, implying that the doping concentration with x = 0.125 is preferable for the photocatalytic performance of doped STO.

4. Conclusions

In summary, the spin-polarized first principles calculation is performed on the electronic structure, magnetic and optical properties of (Fe, Mn) co-doped $SrTiO_3$ with varying doping concentrations. It is revealed that there exhibits a AFM to FM phase transition with increasing doping concentration. A magnetic half-metallic character is found in doped STO (STFMO) with the doping concentration x = 0.25, which is ascribed to the excitation of the O-2p states into the conduction band. The in-gap electric states from Mn-3d states and near neighbor O-2p states induce a reduced band gap, and there only exists strong hybridization between Mn-3d states and O-2p states in gap. The doping concentrations have great influence on the magnetic moments of Fe and Mn atoms. The calculated magnetic moment of Fe is decreases with the doping concentration increases, oppositely, the magnetic moment of Mn is increases with increasing doping concentration. For the doped STO, the calculated static refractive index $n(0)$ is increases with increasing doping concentration. The calculated optical absorption coefficient $\alpha(\omega)$ implies that the doped STO have better photocatalytic performance as the doping concentration is x = 0.125.

Acknowledgements

This work was financially supported by the Postdoctoral Science Foundation of China (2014M550337), the Academic Funding Project for the Top Talents of Colleges and Universities (Grant Nos. gxbjZD14), and the Key Technologies R&D Program of Anhui Province of China (1604a0802122, 17030901091).

References

[1] M. Imada, A. Fujimori, Y. Tokura, Rev. Mod. Phys. **70**, 1039 (1998).
[2] Y. Liu, Q. Qian, J. J. Li, X. G Zhu, M. X. Zhang, T. S. Zhang, J. Nanosci. Nanotech. **16**, 12321 (2016).
[3] Z. Wang, M. Gao, Z. Yao, G Li, Z. Song, W. Hu, H. Hao, H. Liu, Z. Yu, Ceram. Int. **40**, 929 (2014).
[4] F. Zou, Z. Jiang, X. Q. Qin, Y. X. Zhao, L. Y. Jiang, J. F. Zhi, T. C. Xiao, P. P. Edwards, Chem. Commun. **48**, 8514 (2012).
[5] Y. H. Huang, H. B. Lu, H. Z. Guo, L. F. Liu, M. He, Z. H. Chen, Y. L. Zhou, K Zhao, K. J. Jin, J. Z. Yang, Chin. Sci. Bull. **51**, 2035 (2006).
[6] Y. G Zhang, J. F. Hu, E. S. Cao, L. Sun, H. W. Qin, J. Magn. Magn. Mater. **324**, 1770 (2012).
[7] J. H. Haeni, P. Irvin, W. Chang, R. Uecker, P. Reiche, Y. L. Li, S. Choudhury, W. Tian, M. E. Hawley, B. Craigo, A. K. Tagantsev, X. Q. Pan, S. K. Streiffer, L. Q. Chen, S. W. Kirchoefer, J. Levy, D. G. Schlom, Nature **430**, 758 (2004).
[8] M. Muralidharan, V. Anbarasu, A. E. Perumal, K. Sivakumar, J. Mater. Sci.: Mater. Electro. **25**, 4078 (2015).
[9] W. Zheng, L. Zhang, Y. Lin, Z. Shi, F. Cao, G Yuan, J. Mater. Sci.: Mater. Electro. **27**, 12067 (2016).
[10] V. V. Lemanov, Ferroelectrics **226**, 133 (1999).
[11] A. S. Kumar, P. Suresh, M. M. Kumar, H. Srikanth, M. L. Post, K. Sahner, R. Moos, S. Srinath, J. Phys.: Confer. Series **200**, 092010 (2010).
[12] V. Matjaz, K. Taras, A. Iztok, A. Frederic, A. Anna-Karin, N. M. Alford, Adv. Funct. Mater. **22**, 2114 (2012).
[13] M. Muralidharan, V. Anbarasu, A. E. Perumal, K. Sivakumar, J. Mater. Sci.: Mater. Electro. **26**, 6875 (2015).
[14] W. Zhang, H. P. Li, W. Pan, Key Eng. Mater. **512-515**, 1438 (2012).
[15] A. Karaphun, S. Hunpratub, E. Swatsitang, Microelectro. Eng. **126**, 42 (2014).
[16] G. P. Das, B. K. Rao, P. Jena, Phys. Rev. B **68**, 035207 (2003).
[17] M. Kabir, A. Mookerjee, D. G. Kanhere, Phys. Rev. B **73**, 224439 (2006).
[18] D. Choudhury, B. Pal, A. Sharma, S. V. Bhat, D. D. Sarma, Sci. Rep. **3**, 1433 (2013).
[19] T. Shen, C. Hu, H. L. Dai, W. L. Yang, H. C. Liu, C. L. Tan, X. L. Wei, Optik **127**, 3055 (2016).
[20] D. Z. Li, C. Barreteau, A. Smogunov, Phys. Rev. B **93**, 144405 (2016).
[21] M. Segall, M. Probert, C. Pickard, P. Hasnip, S. Clark, K. Refson, J. R. Yates, M. Payne, Z. Fur kristallogr. **220**, 567 (2005).
[22] T. R. Paudel, S. S. Jaswal, E. Y. Tsymbal, Phys. Rev. B **85**, 104409 (2012).
[23] Z. P. Hu, H. Metiu, J. Phys. Chem. C **115**, 5841(2011).
[24] H. L. Shi, M. F. Chu, P. Zhang, J. Nucl. Mater. **400**, 151 (2010).
[25] M. Zeng, S. W. Or, W. H. Chan, J. Appl. Phys. **107**, 043513 (2010).
[26] X. Zhou, J. Y. Shi, C. Li, J. Phys. Chem. C **115**, 8305 (2011).
[27] N. B. Mahmood, E. K. Alshakarchi, B. Elouadi, J. Mod. Phys. **2**, 1420 (2011).
[28] D. Baüerle, W. Braun, V. Saile, G Sprüssel, E. E. Koch, Z. Physik B **29**, 179 (1978).
[29] K. W. Blazey, Phys. Rev. Lett. **27**, 146 (1971).

*Corresponding author: yueqin@mail.ustc.edu.cn
yinliu@aust.edu.cn